Large eddy simulation of high-pressure ECN Spray A with the focus on the influence of injection pressure

Mohammadmahdi Ghiji[1], Fatemeh Salehi[2,*], Longfei Chen[3]
[1]Institute of Sustainable Industries and Liveable Cities, Victoria University, Victoria, Australia
[2]School of Engineering, Macquarie University, NSW 2109, Australia
*Corresponding author: fatemeh.salehi@mq.edu.au
[3]School of Energy and Power Engineering, Beihang University, Beijing 100191, China

Abstract
Due to the rapid advancement in high-performance computation (HPC) capacities, detailed numerical simulations are feasible for complex flows at engine conditions. The simulations aim to enhance our understanding of multi-physics phenomena in such flows that will eventually assist the development of new internal combustion technologies with high thermal efficiency and extremely low emission. The current study presents detailed simulations for the Engine Combustion Network (ECN) Spray A at non-reacting conditions to provide a better understanding of the influence of the injection pressure. A hybrid approach is adopted where Large Eddy Simulation (LES) is employed for the gas phase and a Lagrangian particle tracking approach is chosen for the liquid phase. The Kelvin-Helmholtz Rayleigh-Taylor (KHRT) model is used for the break-up while collision and coalescence are neglected. The evaporation rate is computed using the standard Spalding model whereas the Ranz–Marshall correlation is adopted for the heat transfer between the liquid and gas phases. A high-quality mesh is created. The mesh is locally refined to achieve a minimum mesh size of 0.65 of the nozzle diameter (D). The simulations are conducted using OpenFOAM which is an open source object-oriented C++ computational fluid dynamic (CFD) code. The simulations show good agreement with the measurements for both liquid length and vapour penetration at various injection pressures. The mixture fraction field is well captured at the upstream locations while a slight deviation from the measurements is observed further downstream.

Keywords
large eddy simulation (LES); engine combustion network (ECN); Spray A; OpenFOAM.

Introduction

High-pressure compression-ignition engines have been a topic of considerable interest due to their high-power output and thermal efficiency, although, achieving a low level of soot and NOx is still the main challenge in such engines. New compression-ignition engine technologies use fuel lean, low-temperature combustion (LTC) concept to achieve lower combustion temperatures and a longer pre-combustion mixing of the air and fuel that significantly enhances reduction of the emission. However, LTC and other low emission strategies typically result in lower load capabilities. Understanding the complex multi-physics of the combustion process is essential to improve engine technologies.

Due to the recent advancement in computational resources, computational fluid dynamics (CFD) have become favourable tools to analyse the combustion process. The availability of accurate measurements in well-designed experiments is an essential ingredient in validating and developing a reliable numerical tool that eventually assists the development of the next generation of internal combustion engines. In response, an international collaborative platform known as Engine Combustion Network (ECN) [1] has been established to provide close collaborations between modellers and experimentalists on high-pressure sprays. The ECN defines key parameters and boundary conditions for various targets. One of the main ECN targets is known as Spray A which is a single-hole high-pressure *n*-dodecane spray that closely matches the vaporisation and boiling characteristics of diesel fuels. The ECN provides detailed measurements on fuel-air mixing at both non-reacting and reacting conditions, ignition time, flame stabilisation, and soot formation for a range of ambient conditions as well as injection properties to enhance the understanding of complex multi-scale physics in such flows.

Approaches to model turbulent spray flows fall in two broad categories of Eulerian–Eulerian [2, 3] and Eulerian–Lagrangian [4, 5], both of which have been developed for direct numerical simulation (DNS), large eddy simulation (LES) and Reynolds Averaged Navier Stokes (RANS) frameworks. Eulerian approaches describe clouds of droplets by their velocity and concentration fields which are coupled to the carrier flow. On the other hand, Lagrangian approaches assume the liquid phase as discrete elements and track the dynamics of these elements (droplets) which are approximated as evolving points in space. The Eulerian–Eulerian methods are mainly employed to model primary atomisation in dense sprays as they occur in the near-nozzle region of typical fuel sprays [6, 7]. On the other hand, the Lagrangian approaches are better suited for the secondary breakup and dilute spray regions. Details on both methodologies can be found in the reviews provided in [8, 9, 4, 3].

A simple model which is known as the gas-jet model has been also applied to spray flows. In this model, injected liquid fuel replaced by a gaseous jet while mass and momentum flow rates are equal to those in the experimental liquid jet. The model successfully used in both RANS [10, 11, 12] and the LES framework [13, 14] while recent simulations [14] demonstrated that the model failed for conditions where there is an overlap between the flame base

and the liquid phase. There are a few number of studies that employed the Eulerian–Eulerian method to simulate the ECN high-pressure sprays with the focus on primary atomisation and in-nozzle flows [15, 16, 17]. On the other hand, the Lagrangian approach has been widely adopted to study the ECN Spray A in both RANS [18, 19, 20] and LES [21, 22, 23, 24, 25] frameworks. In high-pressure sprays, the liquid core is very short and atomisation occurs quickly. Due to hot ambient conditions, spray evaporates very fast and consequently, it becomes quickly dilute, allowing to use a Lagrangian method for such flows. However, accurate Lagrangian simulation of high-pressure sprays is still challenging, particularly in the concept of the LES. This is mainly due to difficulties with the spray model and the mesh resolution for highly compressible flow. In this study, we aim to analyse the effects of the injection pressure on air-fuel mixing in the high-pressure ECN Spray A using a Lagrangian spray model in the LES framework.

Methodology

A hybrid Eulerian/Lagrangian method is adopted here. The gaseous flow is modelled in an Eulerian framework while the injected fuel is assumed to be in the form of discrete particles. The Eulerian compressible LES simulates the continuity, momentum and enthalpy fields while a Lagrangian scheme is adopted for the discrete particles. The Favre filtered equations for the conservation of carrier phase mass and momentum are

$$\frac{\partial \bar{\rho}}{\partial t} + \frac{\partial \bar{\rho}\tilde{v}_i}{\partial x_i} = \tilde{S}_\rho \tag{1}$$

$$\frac{\partial \bar{\rho}\tilde{v}_i}{\partial t} + \frac{\partial \bar{\rho}\tilde{v}_i\tilde{v}_j}{\partial x_i} = -\frac{\partial \bar{p}}{\partial x_j} + \frac{\partial}{\partial x_i}\left(\tilde{\tau}_{ij} - \tau_{ij}^{\mathrm{sf}}\right) + \tilde{S}_{v_i}, \tag{2}$$

where v_i, ρ and p are the carrier velocity in the i-direction, density and pressure, respectively. S_ρ and S_{v_i} are the source terms representing effects of dispersed phase on the carrier phase. Overbars and tildes denote Reynolds and Favre filters. In the above, $\tilde{\tau}_{ij}$ is the resolved viscous stress tensor and τ_{ij}^{sf} denotes the unclosed residual-stress tensor which is modelled using the eddy-viscous model [26].
The energy equation is written as

$$\frac{\partial \bar{\rho}\tilde{h}}{\partial t} + \frac{\partial \bar{\rho}\tilde{v}_i\tilde{h}}{\partial x_i} = -\frac{D\bar{p}}{Dx_j} + \frac{\partial}{\partial x_i}\left(\tilde{v}_i\tilde{h} - \tilde{v_i h} + \frac{\bar{\lambda}}{\bar{c_p}}\frac{\partial \tilde{h}}{\partial x_i}\right) + \tilde{S}_h, \tag{3}$$

where h is enthalpy, $\bar{\lambda}$ is the conductivity and $\bar{c_p}$ is the heat capacity. S_h is the source term due to the evaporation.
The liquid phase is presented by a set of computational parcels, each one of them being representative of identical droplets. It is worth noting that the primary atomisation is neglected here while a standard blob model is adopted assuming that the mist consists of small droplets that are below the supercritical temperatures. The initial droplet distribution somehow must be estimated. Following previous studies [21, 22, 23], the Rosin-Rammler distribution function is adopted to obtain the initial diameter of the injected droplets. The main challenge is then to estimate the maximum and minimum values for the initial droplet size distribution. These values are selected as $d_{max} = 18\mu m$ and $d_{min} = 1\mu m$, respectively, which are 1/5 and 1/90 of the nozzle diameter. These choices are based on the recommendation given in [22]. The computed values ensure that the size range corresponds to an unstable regime where the maximum Weber number range is high enough for rapid secondary atomisation near the injection position [27]. The droplet size range is also large enough that the droplets do not evaporate immediately. The droplet velocity is determined by the mass injection profile provided by the experiment.
Assuming the drag is the dominant accelerating force on the droplets, the stochastic Lagrangian equations are written as [28]

$$d\boldsymbol{X} = \boldsymbol{U}dt, \tag{4}$$

$$d\boldsymbol{U} = \frac{1}{\tau_p}\left(\boldsymbol{v} - \boldsymbol{U}\right)dt, \tag{5}$$

where $\boldsymbol{X}$ is the parcel position and $\boldsymbol{U}$ is the velocity. $\boldsymbol{v}$ is the instantaneous career velocity at the particle location. Here, the subgrid effects are neglected as the large scale velocities are dominant and hence $\boldsymbol{v}$ is estimated at the particle location by tri-linear interpolation from the three-dimensional finite volume resolved velocities obtained from Eq. 2. τ_p is the response time due to carrier and dispersed phase interaction forces and it is modelled as

$$\frac{1}{\tau_p} = \frac{1}{2}C_D\frac{\rho}{\rho_d}\frac{A_d}{V_d}|\boldsymbol{v} - \boldsymbol{U}|, \tag{6}$$

where C_D is the drag coefficient, ρ is the carrier fluid density, ρ_d is the dispersed phase density, A_d is a reference area (usually droplet projected area) and V_d is the droplet volume. The drag coefficient for spherical droplets is expressed as

$$C_D = \begin{cases} \frac{24}{Re}(1 + 0.15(Re^{2/3})) & \text{Re < 1000} \\ C_D^{\text{crit}} & \text{Re > 1000} \end{cases} \tag{7}$$

Re is defined as $2\rho|\boldsymbol{U} - \boldsymbol{v}|r/\mu$ where r is the droplet radius and μ is the carrier fluid viscosity. $C_D^{\text{crit}} = 0.424$ is the critical drag coefficient [29].
The combined Kelvin-Helmholtz/Rayleigh-Taylor (KH-RT) breakup model [30] is adopted here. The Kelvin–Helmholtz and Rayleigh–Taylor instabilities are the fundamental mechanisms that govern the breakup. The Kelvin–Helmholtz (KH) model assumes the growth of an initial perturbation on a droplet surface is related to its wavelength while the Rayleigh–Taylor (RT) model represents the second type of instability associated with the rapid deceleration of droplets due to the drag force. Based on the KH model, the radius of a newly created droplet, $r_{c,KH}$ is given by $B_0\Lambda_{KH}$ where $\mathrm{B}_0 = 0.61$ is the model constant and Λ_{KH} is the wavelength [18]. The change of droplet's radius is determined as

$$\frac{dr}{dt} = -\frac{r - r_{c,KH}}{\tau_{KH}}, \tag{8}$$

where τ_{KH} is the KH breakup characteristic time and it is computed using

$$\tau_{KH} = 3.76\frac{B_1 r}{\Lambda_{KH}\Omega_{KH}}, \tag{9}$$

where $B_1 = 5$ is the model constant [21] and Ω_{KH} represents the frequency of the fastest-growing wave. On the other hand, the RT model assumes the RT waves grow on the surface if the RT wavelength, Λ_{RT}, is smaller than the droplet radius. Λ_{RT} is defined as $2\pi C_{RT}/K_{RT}$ where $C_{RT} = 0.1$ is the RT model constant and K_{RT} is the wave number. With the initiation of a RT wave, their lifetime is tracked and the droplet will experience the breakup if the lifetime of the RT wave exceeds the characteristic RT time scale. Unstable waves are allowed to simultaneously grow in both models. If the RT model predicts a break-up within the actual time step, the RT mechanism is the driven model for the droplet disintegration. Otherwise, child droplets are produced by the KH model that simultaneously reduces the diameter of the parent droplet.
Droplet evaporation rate is obtained using the droplet size and Spalding and Nusselt numbers in which the Ranz–Marshall correlation is adopted for the heat transfer between the liquid and gas phases [31]. Collision and coalescence are assumed to be negligible due to their small influence in evaporating sprays [18].

Experimental and numerical setup

The ECN Spray A consists of *n*-dodecane issuing from a single-hole injector with a diameter of 90 μm into a constant-volume cubic chamber of 108 mm sides. The present work use the experimental data provided by Sandia National Laboratory (SNL) and CMT-Motores [1]. CMT-Motores employs a Constant-Pressure Flow Test Rig (CPF) while SNL uses Constant Volume Pre-burn (CVP). The ambient temperature is 900 K whereas the ambient pressure is 6 MPa. The ambient density is 22 kg/m^3 and the ambient oxygen volume fraction is 0% representing non-reacting conditions. The fuel injection density and temperature are kept as 713 kg/m^3 and 363 K while the fuel injection pressure varies between 50 and 150 MPa.
The computational domain covers 60 mm in the axial length of the chamber and it is partially extended in other directions. The domain length in both transverse directions is about one third of the chamber size at the top where the injector is mounted and two third of the chamber size at the bottom. The selected domain is large enough to ensure that the boundaries do not affect the jet development while significantly reduces the computational cost. Free stream boundary conditions are applied along these directions. The mesh is refined by a 2:1 cell-splitting approach in the spray region. The minimum cell size is 58 μm which is corresponding to 0.65 of the nozzle diameter, and the total number of computational cells is approximately 5 millions. It is worth noting that maintaining a similar mesh resolution would result in the total number of cells of about 20 millions if the computational domain covered full length in axial and transverse directions. The mesh resolution is consistent with the previous LES studies of Spray A [22, 23, 25].
The simulations are performed using OpenFOAM 4.x which is a C++ open source CFD package. Both standard Smagorinsky and the one-equation eddy viscus models were tested for the base case with the injection pressure of 150 MPa. The results confirmed the difference between these subgrid models was small and the former was adopted for all simulations. A pressure-implicit algorithm with the splitting of operators (PISO) is employed to treat the pressure-velocity coupling. The LES uses an implicit, second-order temporal and second-order spatial discretisation schemes. Linear Guess is used to discretising the diffusion term. Both Gamma and limitedLinear schemes were tested for the convection term. Although both methods were stable, limitedLinear provided better agreement with the measurements and its results are presented here.

The total injected fuel mass is computed by integration of the fuel mass profiles (given by the experiment) over the injection duration which is 1.5 ms. It results in 1.92, 2.81 and 3.46 mg of fuel for 50, 100 and 150 MPa, respectively. The amount of injected mass at each time step is then computed as a fraction of the total mass. The diameter of injected droplets is obtained from the given Rosin-Rammler size distribution. OpenFOAM uses a numerical parameter known as parcelPerSecond to control the number of injected parcels. Consequently, the number of droplets per parcel can be obtained. The mass of injected parcel which depends on the number of droplets per parcel is a critical parameter in LES-Lagrangian method. Obviously, decreasing parcelPerSecond reduces the number of injected parcels at each time step and hence decreases the computational cost. However, it increases the parcel mass. Heavy parcels may cause instability in the solution since they introduce a sudden jump in the density field due to a large rate of evaporation. Here, we used 50×10^6 parcelPerSecond for the simulations. Parcels are injected with an axial location of zero whereas their locations at transverse directions are randomly selected on the nozzle area.

Results and discussion

Figure 1 illustrates instantaneous contours of mixture fraction at 0.25, 0.5, 0.75 and 1 ms after the start of injection for different injection pressures. The time increases from top to bottom while the injection pressure increases from left to right. For the considered instants, the jet base does not change as the jet evolves and it is not sensitive to the injection pressure. At higher injection pressures, rates of droplet size reduction due to breakup and evaporation are expected to be increased, and this nearly cancels with the increased initial droplet momentum. Consequently, the jet base becomes insensitive to injection pressure. As the injection pressure increases, the vapour fuel penetrates further downstream into the domain.

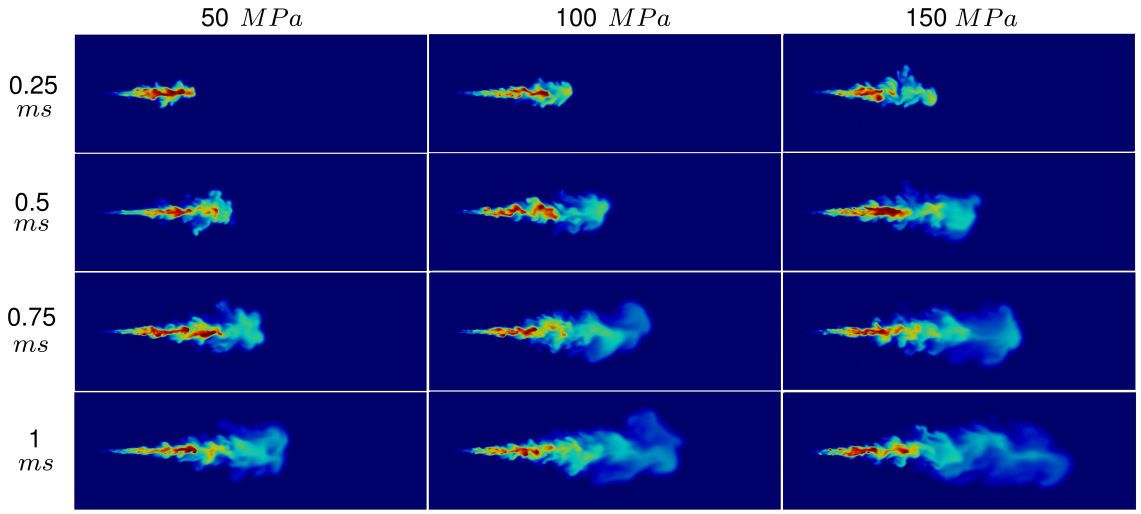

Figure 1. Instantaneous vapour fuel at t = 0.25, 0.5, 0.75 and 1 ms from top to bottom. The first, second and third columns are corresponding to the injection pressure of 50, 100 and 150 MPa, respectively.

Figure 2 presents the liquid and vapour penetration lengths for the injection pressure of 50, 100, and 150 Mpa. The simulations are presented by lines while the experimental data are presented by symbols. The liquid penetration length is calculated as the axial distance covering 95% of the injected liquid fuel mass and the vapour penetration length is measured as the maximum distance from the nozzle tip to the location where the fuel mass fraction is 0.1% of its maximum values. It can be seen that the simulated liquid penetration length agrees well with the measurements for the injection pressure of 100 and 150 MPa while it slightly deviates from the experimental data for the case with the lowest injection pressure. Similar to the experimental data, the liquid length is marginally sensitive to the injection pressure which is consistant with the observations in Fig. 1. It is expected decreasing the injection pressure slightly increases the liquid penetration length although as mentioned, this is compensated by the change in overall evaporation rate, which is controlled by the air-entrainment and hence the sensitivity of the liquid length to the injection pressure is small [32]. The simulations show that the liquid length achieves to the quasi-steady state at about 0.21 ms after the start of injection which is close to the value (0.22 ms) reported by the experiment. The LES results for vapour penetration length agree very well with the measurements at the injection pressure of 50 and 100 MPa while the LES results reveal slight over-predictions compared to the experimental data for the highest injection pressure after 1 ms after the start of injection.

Radial profiles of azimuthally averaged mixture fraction at locations 20 mm and 30 mm downstream of the nozzle exit are shown in Fig. 3. The predicted values are shown for a time after the quasi-steady jet condition has been reached. For 50 and 100 MPa, the LES results show good agreement with the experimental data at 30 mm where the centreline values and radial dispersion of the jet are accurately captured. The computed centreline mixture fraction is under predicted at 150 MPa while its radial span is well predicted. At 20 mm, the centreline value is slightly over-predicted for the case with the injection pressure of 50 MPa while it is captured well for higher injection

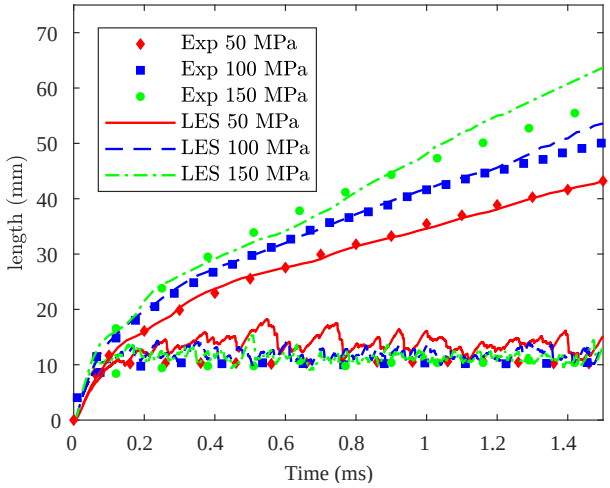

Figure 2. Liquid and vapour penetration lengths; solid lines, LES; symbols, measurements.

pressures. The simulations confirm the spray model parameters have a significant impact on the results. Although we tested various values for spray model constants here, a systematic study is still required to highlight effects of each parameter.

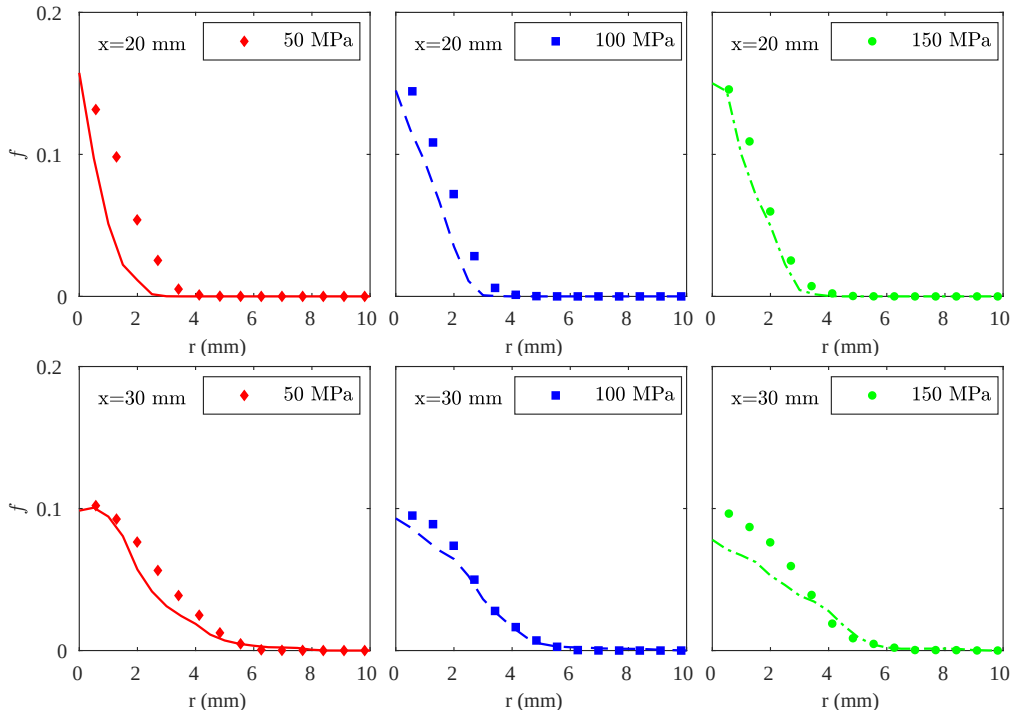

Figure 3. Radial profiles of the mixture fraction at the axial locations of 20 and 30 mm for cases with the injection pressure of 50, 100 and 150 MPa.

Conclusions

The ECN spray A at non-reacting conditions was modelled using the LES approach while a Lagrangian method was adopted for the evolution of liquid droplets. The simulation results were compared with the available experimental data, including liquid and vapour penetration lengths, instantaneous mixture fraction profiles, and radial profiles of the mixture fraction. The effect of injection pressures on spray characteristics was also analysed. The LES results showed satisfactory agreement with the measurements at considered pressure injections. It was found an increase in the injection pressure enhanced the vapour penetration length while its impact was small on the liquid penetration length. Although good agreement was achieved, a detailed analysis is still essential to understand the atomisation model behaviour and its influence on the vapour field which will be considered in out future work.

Acknowledgements
The authors acknowledge the AWS service funded by Macquarie University for providing computing resources.

References

[1] (http://www.sandia.gov/ecn/index.php).

[2] O. Desjardins, V. Moureau, H. Pitsch, J. Comput. Phys. 227 (2008) 8395 – 8416.

[3] K. Luo, C. Shao, M. Chai, J. Fan, Prog. Energy Combust. Sci. 73 (2019) 65 – 94.

[4] S. Subramaniam, Progr. Energy Combust. Sci. 39 (2013) 215–245.

[5] F. Salehi, M. J. Cleary, A. R. Masri, J. Fluid Mech. 831 (2017) 719–742.

[6] M. Ghiji, L. Goldsworthy, P. Brandner, V. Garaniya, P. Hield, Fuel 175 (2016) 274 – 286.

[7] M. Ghiji, L. Goldsworthy, P. Brandner, V. Garaniya, P. Hield, Fuel 188 (2017) 352 – 366.

[8] S. Balachandar, J. K. Eaton, Ann. Rev. Fluid Mech. 42 (2010) 111–133.

[9] X. Jiang, G. A. Siamas, K. Jagus, T. G. Karayiannis, Prog. Energy Combust. Sci. 36 (2010) 131–167.

[10] J. Abraham, L. M. Pickett, Atomization Sprays 20 (2010).

[11] C. Bajaj, J. Abraham, L. M. Pickett, Atomization Sprays 21 (2011).

[12] Y. Pei, E. R. Hawkes, S. Kook, Proc. Combus. Inst. 34 (2013) 3039–3047.

[13] F. Salehi, M. J. Cleary, A. R. Masri, SAE Paper 2016-01-0859, 2016.

[14] F. Salehi, M. J. Cleary, A. R. Masri, Y. Ge, A. Y. Klimenko, Proc. Combust. Inst. 36 (2017) 3577–3585.

[15] S. Som, S. Aggarwal, Combust. Flame 157 (2010) 1179 – 1193.

[16] Q. Xue, M. Battistoni, C. Powell, D. Longman, S. Quan, E. Pomraning, P. Senecal, D. Schmidt, S. Som, Int. J. Multiphase Flow 70 (2015) 77 – 88.

[17] J. Matheis, S. Hickel, Int. J. Multiphase Flow 99 (2018) 294 – 311.

[18] G. D'Errico, T. Lucchini, F. Contino, M. Jangi, X.-S. Bai, Combust. Theor. Model. 18 (2014) 65–88.

[19] Y. Pei, E. R. Hawkes, S. Kook, G. M. Goldin, T. Lu, Combust. Flame 162 (2015) 2006–2019.

[20] M. A. Chishty, M. Bolla, E. R. Hawkes, Y. Pei, S. Kook, Combust. Flame 192 (2018) 101 – 119.

[21] Q. Xue, S. Som, P. K. Senecal, E. Pomraning, Atomization Sprays 23 (2013) 925–955.

[22] A. Wehrfritz, V. Vuorinen, O. Kaario, M. Larmi, Atomization and Sprays 23 (2013) 419–442.

[23] H. Kahila, A. Wehrfritz, O. Kaario, M. G. Masouleh, N. Maes, B. Somers, V. Vuorinen, Combust. Flame 191 (2018) 142 – 159.

[24] C. Xu, M. M. Ameen, S. Som, J. H. Chen, Z. Ren, T. Lu, Combust. Flame 195 (2018) 30 – 39.

[25] Y. Pei, S. Som, E. Pomraning, P. K. Senecal, S. A. Skeen, J. Manin, L. M. Pickett, Combust. Flame 162 (2015) 4442 – 4455.

[26] V. Raman, H. Pitsch, Proc. Combus. Inst. 31 (2007) 1711–1719.

[27] G. Stiesch, Modeling engine spray and combustion processes, Springer Science & Business Media, 2003.

[28] M. R. Maxey, J. J. Riley, Phys. Fluids (1958-1988) 26 (1983) 883–889.

[29] E. Loth, Powder Technol. 182 (2008) 342–353.

[30] R. REITZ, et al., Atomisation and Spray Technology 3 (1987) 309–337.

[31] W. Ranz, W. R. Marshall, et al., Chem. eng. prog 48 (1952) 141–146.

[32] D. L. Siebers, SAE Transactions (1998) 1205–1227.